

Effects of La-substitution on the magnetic properties of the $\text{Ba}_{1-x}\text{La}_x(\text{Ti}_{1/2}\text{Mn}_{1/2})\text{O}_3$ ($x = 0.0, 0.1$) 12R-type Perovskite.

F. A. Garcia,^{1,2} P. Marques-Ferreira,³ J. G. S. Duque,⁴ D. J. Garcia,⁵ J. Sichelschmidt,¹
P. G. Pagliuso,² N. S. Camilo,³ A. O. García Rodríguez,³ and R. Lora-Serrano³

¹Max Planck Institute for Chemical Physics of Solids, D-01187 Dresden, Germany

²Instituto de Física “Gleb Wataghin”, UNICAMP, 13083-970, Campinas-SP, Brazil

³Instituto de Física, Universidade Federal de Uberlândia, 38400-902, Uberlândia, MG, Brazil

⁴Núcleo de Física, Campus Itabaiana, UFS, 49500-000, Itabaiana, SE, Brazil

⁵Consejo Nacional de Investigaciones Científicas y Técnicas (CONICET)
and Centro Atómico Bariloche, S.C. de Bariloche, Río Negro, Argentina

The magnetic properties and structural details of the 12R-type hexagonal perovskites $\text{BaTi}_{1/2}\text{Mn}_{1/2}\text{O}_3$ and $\text{Ba}_{0.9}\text{La}_{0.1}\text{Ti}_{1/2}\text{Mn}_{1/2}\text{O}_3$ were investigated by means of DC-magnetization, electron spin resonance (ESR) and X-ray diffraction (XRD) experiments. The magnetic data were collected in the temperature (T) interval $2\text{K} \leq T \leq 350\text{K}$. The ESR measurements were performed at both X -band (9.4 GHz) and Q -band (34.4 GHz) frequencies. Our results suggest that the La-substitution on the Ba site induces a field-dependent long range antiferromagnetic ordering of the Mn moments at low-temperature ($T_N = 5\text{K}$) which competes with strong magnetic frustration. Furthermore, we suggest that this frustration is an intrinsic property of the system and is not related with sample inhomogeneities. The XRD data, collected at room temperature, have confirmed the formation of the trigonal perovskite phases in both cases and gives insight on how the magnetic exchange at the Mn/Ti sites (within oxygen octahedra) may vary with La-doping.

PACS numbers:

I. INTRODUCTION

Oxides materials with perovskite structure are outstanding examples of materials used in technological applications, as well as in fundamental studies in condensed matter physics due to the great number of observed ground states such as: multiferroicity, high-temperature superconductivity, colossal magnetoresistive effects and many others.¹ The ideal formula unit is ABO_3 , where A is a rare earth or alkaline earth cation, and B is a smaller transition metal cation like Ti, Mn, Co or Ni. When a second (B') metal atom is added to the above structure, an ordered double perovskites-type structure $\text{A}_2\text{B}'\text{B}''\text{O}_6$ (where $B', B'' = 3d, 4d, 5d$ metals) as well as the disordered $\text{AB}'_{1/2}\text{B}''_{1/2}\text{O}_3$ structure might be formed. One of the challenges in the field of perovskites-type structure based multiferroic materials (where the coexistence of magnetic and electrical orders occurs), for instance, is the enhancement of the coupling between the magnetic and ferroelectric degrees of freedom.² One possible way to add knowledge into this problem may be making “mixed” perovskites with d^0 and d^n ions.³

In this work, we focus on both microscopic and macroscopic magnetic properties of the 12R-type structure perovskites $\text{BaTi}_{1/2}\text{Mn}_{1/2}\text{O}_3$ and $\text{Ba}_{0.9}\text{La}_{0.1}\text{Ti}_{1/2}\text{Mn}_{1/2}\text{O}_3$ (space group $R\bar{3}m$) as a function of temperature ($2\text{K} \leq T \leq 350\text{K}$). The former is a modest dielectric insulator at room temperature with high permittivity $\epsilon_r \sim 45$ (at both radio and microwave frequencies).⁴ In $\text{Ba}_{0.9}\text{La}_{0.1}\text{Ti}_{1/2}\text{Mn}_{1/2}\text{O}_3$, Ba is partially replaced by trivalent La, promoting the coexistence of Mn^{4+} with Mn^{3+} ions at B' and B'' -sites of the $\text{AB}'_{1/2}\text{B}''_{1/2}\text{O}_3$ struc-

ture.

In an attempt of shedding light into the evolution of the magnetic properties of these manganites as a function of the A ion substitution, we report electron spin resonance (ESR), performed at both X -band and Q -band frequencies, along with DC-magnetic susceptibility measurements as a function of temperature and X-ray powder diffraction at room temperature. ESR is a microscopic probe to the Mn spin dynamics and gives valuable information concerning the Mn local site symmetry, sample inhomogeneities and the nature of the exchange interaction. In the particular case of transition-metal-oxides, ESR was shown to be an important probe to both orbital and charge order in many compounds, specially through the analysis of the evolution of the ESR linewidth (ΔH) with temperature, which is a direct measurement of the spin relaxation behavior.⁵⁻¹¹ XRD data in powdered samples combined with Rietveld refinements and bond valence sums calculations, on the other hand, may complement the investigation of the macroscopic, as well as the microscopic, magnetic properties by indicating the atomic arrangement and site occupancy of the atoms responsible for the magnetic exchange.

II. EXPERIMENT

Polycrystalline samples of $\text{Ba}_{1-x}\text{La}_x\text{Ti}_{1/2}\text{Mn}_{1/2}\text{O}_3$ ($x = 0.0$ and 0.1) were synthesized by a simpler synthesis procedure by using a solid state reaction method, that allowed us to obtain good quality samples. Stoichiometric amounts of BaCO_3 , La_2O_3 , MnO_2 and TiO_2 were mixed and grounded in an Agata mortar for five hours

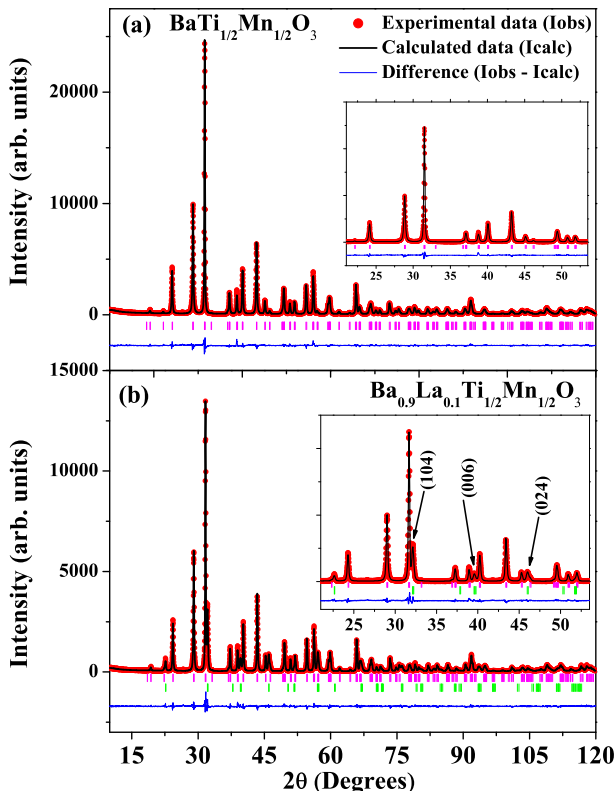


Figure 1: Observed, calculated and difference X-ray diffraction patterns at room temperature of: (a) $\text{BaTi}_{1/2}\text{Mn}_{1/2}\text{O}_3$ and (b) $\text{Ba}_{0.9}\text{La}_{0.1}\text{Ti}_{1/2}\text{Mn}_{1/2}\text{O}_3$ samples, both refined in the trigonal $R\bar{3}m$ space group (hexagonal basis). For the La-substituted sample, superstructure peaks from a secondary rhombohedral phase, $\text{Ba}_{0.4}\text{La}_{0.6}\text{Ti}_{1/2}\text{Mn}_{1/2}\text{O}_3$ (inset), has been included in the refinement (see text).

and heated in air at 900 °C for 24 hours in a conventional tubular furnace. After the first step, the material was re-grounded for thirty minutes and subsequently heated at 1100 °C for 24 hours in air. The X-ray diffraction experiments were performed at room temperature using a Shimadzu XRD6000 diffractometer operating with $\text{Cu-K}\alpha$ radiation and graphite monochromator. Samples were scanned between 10° and 120° in 2θ with a $\Delta 2\theta = 0.02$. The structure refinements were carried out by the Rietveld analysis of the X-ray powder diffraction data at room temperature by using the General Structure Analysis System (GSAS) software.^{12,13} The low-temperature magnetization measurements were performed in a commercial Quantum Design MPMS SQUID magnetometer in the temperature (T) range $2\text{K} \leq T \leq 350\text{K}$, with applied field magnetic field of 1 kOe. The ESR measurements were performed at both X-band (9.4 GHz) and Q-band (34.4 GHz) frequencies using a commercial Bruker Eleksys-500 spectrometer in the temperature interval $4.2\text{K} \leq T \leq 300\text{K}$. The temperature was controlled by using a conventional He flow cryostat.

III. RESULTS AND ANALYSIS

The crystal structure of the 12-R perovskite compound $\text{BaTi}_{1/2}\text{Mn}_{1/2}\text{O}_3$ has been extensively discussed in Refs. 4,14. Here, we just show the results of the Rietveld refinement to the X-ray powder diffraction data of the sample used in this study. Figures 1(a)-(b) show the observed and calculated X-ray powder diffraction data of the (a) $\text{BaTi}_{1/2}\text{Mn}_{1/2}\text{O}_3$ and (b) $\text{Ba}_{0.9}\text{La}_{0.1}\text{Ti}_{1/2}\text{Mn}_{1/2}\text{O}_3$ compounds as obtained from the Rietveld refinement of the experimental data (dotted curve). The data of the non-substituted $\text{BaTi}_{1/2}\text{Mn}_{1/2}\text{O}_3$ compound (Fig. 1(a)) can be indexed in the trigonal $R\bar{3}m$ space group (hexagonal basis) with unit cell parameters $a=5.6845(1)\text{Å}$ and $c=27.8967(6)\text{Å}$ (Table I). The inset in Fig. 1(a) shows a selected region where new reflections appeared for the substituted sample (below). Vertical bars indicate the Bragg peaks positions according to the structural model. The unit cell as reported in Ref. 4 was used as the starting structural model, i.e. considering three different B'/B'' crystallographic sites for Mn^{4+} and Ti^{4+} ions at the face-shared $(\text{Ti,Mn})_3\text{O}_{12}$ trimmers and vertex-shared $(\text{Mn,Ti})\text{O}_6$ octahedra, so-called $M(1)$, $M(2)$ and $M(3)$ ^{4,15} (see Fig. 2). A total of 37 parameters were successfully refined. Refinements of the oxygen concentration did not point to any oxygen-deficiencies, therefore this sample can be considered oxygen stoichiometric. In addition, no secondary phases were observed within the resolution of our XRD experiments. The goodness-of-fit parameters R_p , R_{wp} and χ^2 are consistent with a good agreement between the structural model and the experimental data (Table I).

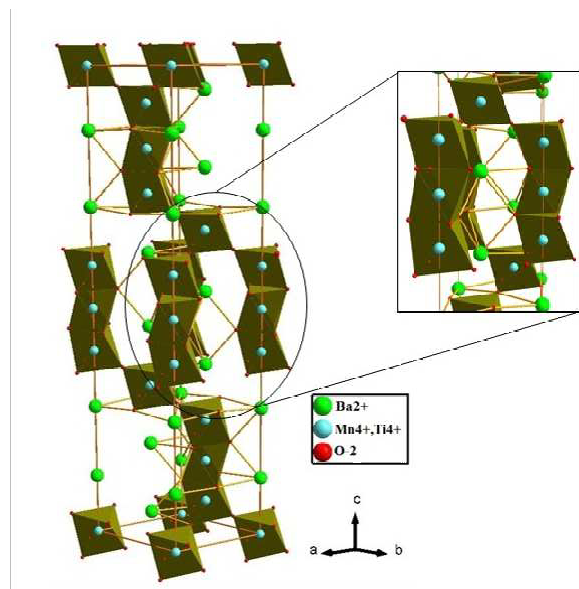


Figure 2: (Color online) 3D view¹⁶ of the 12R-type unit cell highlighting the (Ti,Mn) face- and corner shared octahedra (B site cation arrangement). For detailed oxygen positions, refer to figure 8 of Ref. 4.

Table I: Unit cell parameters (in Å), goodness-of-fit parameters and selected interatomic distances (in Å) and angles (in degrees) extracted from the Rietveld refinements of $\text{BaTi}_{1/2}\text{Mn}_{1/2}\text{O}_3$ and $\text{Ba}_{0.9}\text{La}_{0.1}\text{Ti}_{1/2}\text{Mn}_{1/2}\text{O}_3$. Numbers between parenthesis are errors of the last significant digit.

Sample	$\text{BaTi}_{1/2}\text{Mn}_{1/2}\text{O}_3$	$\text{Ba}_{0.9}\text{La}_{0.1}\text{Ti}_{1/2}\text{Mn}_{1/2}\text{O}_3$
Crystal structure	Trigonal	Trigonal
Space group	$R\bar{3}m$	$R\bar{3}m$
a	5.6845(1)	5.6862(1)
c	27.8967(6)	27.9149(6)
Volume (Å ³)	780.66(3)	781.64(3)
R_p (%)	9.01	9.48
R_{wp} (%)	6.47	6.84
χ^2	3.01	2.02
Ba(1)–O(2)×6	2.8491(6)	2.8490(7)
Ba(1)–O(2)×3	2.946(10)	2.957(13)
Ba(2)–O(1)×6	2.8516(5)	2.8557(6)
Ba(2)–O(1)×3	2.904(6)	2.947(7)
Ba(2)–O(2)×3	2.957(10)	2.948(13)
Ba(1)–O(1)×3	2.801(6)	2.809(6)
M(1)–O(1)×6	1.895(6)	1.87310(2)
M(2)–O(1)×3	1.998(6)	1.94744(2)
M(2)–O(2)×3	1.922(9)	1.88922(2)
M(3)–O(2)×6	1.969(9)	2.00260(2)
M(1)–M(2)	2.566(4)	2.56929(5)
M(2)–M(3)	3.893(9)	3.8918(2)
M(1)–O(1)–M(2)	82.41(25)	84.496(1)
M(2)–O(2)–M(3)	175.5(6)	174.971(1)

Considering the small difference between the X-ray atomic scattering factors of manganese and titanium, the population at the B'/B'' sites was kept fixed (0.5/0.5) during the refinement. Therefore, in order to know the occupation of the B sites, bond valence sum (BVS) calculations (Table II) for the B -O bonds were performed by using the SPuDS simulation software¹⁷ and the bond lengths obtained from XRD refinements (Table I). The Ti^{4+} and Mn^{4+} configurations were assumed in both cases. From BVS results it becomes evident that Mn ions have preference for the inner $M(1)$ sites of the face shared octahedra, whereas Ti ions are preferentially allocated in the corner shared octahedra $M(3)$ sites and in the outer sites of the face shared octahedra [$M(2)$], sharing the latter with Mn ions. According to these results, the proposed cationic distribution is $\text{Ba}(\text{Mn}_{0.25}^{4+})_{M(1)}(\text{Ti}_{0.25}^{4+}\text{Mn}_{0.25}^{4+})_{M(2)}(\text{Ti}_{0.25}^{4+})_{M(3)}\text{O}_3$, which is in agreement with Ref. 4.

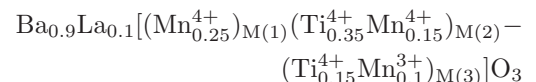
When 10% of Ba^{2+} is substituted by La^{3+} at the A -site of the $\text{BaTi}_{1/2}\text{Mn}_{1/2}\text{O}_3$ compound, the $\text{Ba}_{0.9}\text{La}_{0.1}\text{Ti}_{1/2}\text{Mn}_{1/2}\text{O}_3$ compound is formed. In order to account for the structural details of this new compound, we also used as the starting model the unit cell of $\text{BaTi}_{1/2}\text{Mn}_{1/2}\text{O}_3$ system,⁴ now by adding the La atoms preferentially to one of the Ba 6c sites; the best results were obtained with this configuration and, as it is physically plausible, it was assumed for the unit cell. Fig. 1(b) shows the observed, calcu-

Table II: Bond Valence Sums for Ti and Mn in $\text{BaTi}_{1/2}\text{Mn}_{1/2}\text{O}_3$ and $\text{Ba}_{0.9}\text{La}_{0.1}\text{Ti}_{1/2}\text{Mn}_{1/2}\text{O}_3$. B^{3+} and B^{4+} indicate the valence used in the calculations.

Sample		M Sites		
		M(1)	M(2)	M(3)
$\text{BaTi}_{1/2}\text{Mn}_{1/2}\text{O}_3$	$(\text{Mn}^{4+}) \sum V_{\text{Mn-O}}$	4.09	3.45	3.34
	$(\text{Ti}^{4+}) \sum V_{\text{Ti-O}}$	4.83	4.08	3.95
$\text{Ba}_{0.9}\text{La}_{0.1}\text{Ti}_{1/2}\text{Mn}_{1/2}\text{O}_3$	$(\text{Mn}^{4+}) \sum V_{\text{Mn-O}}$	4.34	3.85	3.06
	$(\text{Ti}^{4+}) \sum V_{\text{Ti-O}}$	4.42	3.93	3.11
		5.13	4.55	3.61

lated and difference XRD data for the $x=0.1$ sample. The calculated cell parameters are $a=5.6861(1)\text{Å}$ and $c=27.9151(5)\text{Å}$. In addition to the peaks from the main phase, new reflections were also observed. Our Rietveld analysis reveals that the new peaks can be associated to a new secondary phase, with stoichiometry $\text{Ba}_{0.4}\text{La}_{0.6}\text{Ti}_{1/2}\text{Mn}_{1/2}\text{O}_3$ ($R\bar{3}c$ space group) and lattice parameters $a=5.6127(2)\text{Å}$ and $c=13.7004(13)\text{Å}$, which occupies roughly 17% of the overall volume. The inset in Fig.1(b) presents the same selected 2θ region as in Fig.1(a), but here we show with arrows some of the reflections from the second phase. Vertical bars represent the angular positions of the Bragg peaks from both crystalline phases (top bars: main phase; bottom bars: secondary phase). Other possible phases such as LaMnO_3 (trigonal structure), $\text{Ba}_{0.5}\text{La}_{0.5}\text{Ti}_{1/2}\text{Mn}_{1/2}\text{O}_3$ (tetragonal) and $\text{Ba}_{0.3}\text{La}_{0.7}\text{Ti}_{1/2}\text{Mn}_{1/2}\text{O}_3$ (trigonal) were also tested, however, the best fit to the data was obtained by using the unit cell of the $\text{Ba}_{0.4}\text{La}_{0.6}\text{Ti}_{1/2}\text{Mn}_{1/2}\text{O}_3$ compound as the secondary phase.

With the La-substitution the total charge compensation requires that electrons, holes, or vacancies to be produced, and this may change transport and magnetic properties of these materials.¹⁸ Depending on the total amount of trivalent lanthanum, or divalent barium at the A site, manganese at the B site may be in 3+ or 4+ oxidation states. However, if oxygen deficiency is present, the expected proportion of $\text{Mn}^{3+}/\text{Mn}^{4+}$ could be different from the ideal ratio due to the negative charge compensation.¹⁹ From our Rietveld refinement results, no oxygen deficiencies were obtained for the main phase nor for the secondary phase. In addition, BVS calculations assuming Ti^{4+} , Mn^{3+} and Mn^{4+} configurations for the main phase (Table II) suggest that $M(1)$ will be fully occupied by Mn^{4+} ions, while $M(2)$ sites will be occupied by Mn^{4+} and Ti^{4+} ions and $M(3)$ sites will be shared by Mn^{3+} and Ti^{4+} , as expected from a higher $M(3)$ -O distance. From this analysis, the proposed cationic distribution for this sample can be,



In Fig. 3 we show representative X -band and Q -band ESR spectrum lines for both samples. The spectra con-

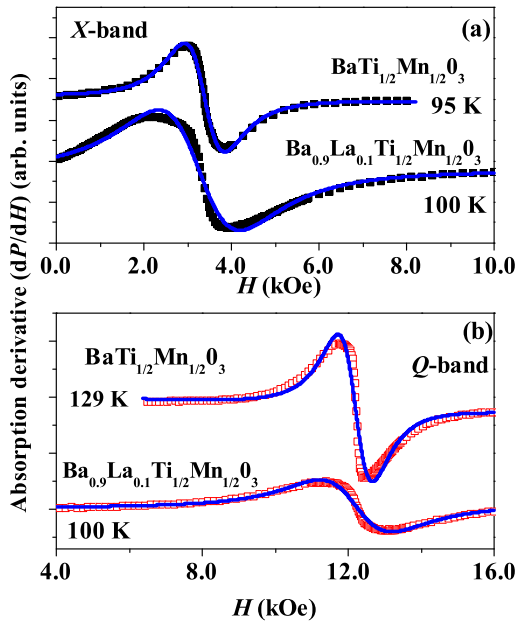


Figure 3: (color online) Representative ESR spectra measured for $\text{BaTi}_{1/2}\text{Mn}_{1/2}\text{O}_3$ and $\text{Ba}_{0.9}\text{La}_{0.1}\text{Ti}_{1/2}\text{Mn}_{1/2}\text{O}_3$ at (a) X-band and (b) Q-band frequencies. The solid line is the best fitting of the data to a Lorentzian lineshape.

sist of *exchange narrowed* broad lines, typical of concentrated paramagnetic systems. The solid line represent the fitting of the data to a Lorentzian lineshape, as appropriate for an insulator host, which also takes into account corrections due to the effects of the counter resonance for broad ESR lines.²⁰ In our work, the quantities of interest of the ESR experiment are the linewidth (ΔH), roughly the peak-to-peak distance in the field scale of the observed spectra, and the g -values, which are obtained from the resonance condition ($h\nu = g\mu_B H_{\text{res}}$, where H_{res} is the resonance field).

For $\text{BaTi}_{1/2}\text{Mn}_{1/2}\text{O}_3$ the goodness of the fitting can be verified by direct inspection of Fig. 3. However, for the $x = 0.1$ sample, the lineshape deviates from the expected Lorentzian lineshape, suggesting that these spectra are composed by more than one contribution. Indeed, in this case the best fit to the data was obtained by using two Lorentzian lines, which we tentatively ascribe to contributions originated from the main phase and the secondary phase observed in XRD experiments (see Fig.1). However, we could not extract out of the fitting process a systematic behavior to deconvolute these contributions. Nevertheless, we could determine that for $T < 50\text{K}$ the ESR response is dominated by the secondary phase and by the main phase otherwise.

Furthermore, as we shall discuss below, the resonance of both samples was found to be homogeneous, i.e. ΔH is not broadened due to some inhomogeneous field distribution in the sample (disorder effects, etc). Hence, the measured spectra and its behavior as a function of temperature (T) and field (H), can be taken as a probe of

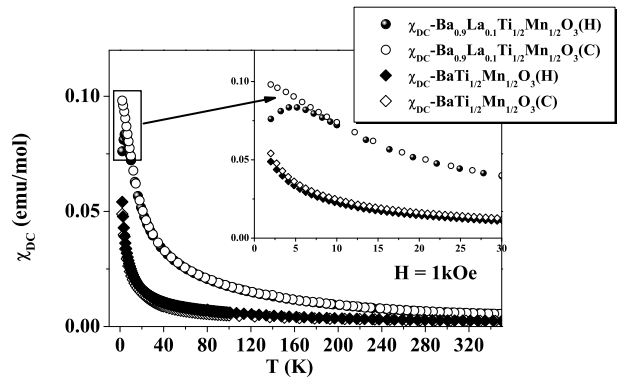


Figure 4: Temperature dependence of the DC-susceptibility in an applied magnetic field of 0.1 T in the zero field cooling and field cooling (ZFC-FC) regimes for $\text{BaTi}_{1/2}\text{Mn}_{1/2}\text{O}_3$ and $\text{Ba}_{0.9}\text{La}_{0.1}\text{Ti}_{1/2}\text{Mn}_{1/2}\text{O}_3$. “H” and “C” in legends stand for Heating and Cooling regimes, respectively.

the intrinsic properties of both systems.

In figure 4 we present the field-cooled and zero-field-cooled DC-susceptibility χ_{DC} (open and filled symbols, respectively), for $\text{BaTi}_{1/2}\text{Mn}_{1/2}\text{O}_3$ and $\text{Ba}_{0.9}\text{La}_{0.1}\text{Ti}_{1/2}\text{Mn}_{1/2}\text{O}_3$. It is shown that our χ_{DC} vs. T data does not show a typical Curie-Weiss behavior for all the studied temperature range. From the linear fitting to the χ_{DC}^{-1} data taken at the highest temperatures available, we extracted the effective magnetic moment μ_{eff} and the Curie-Weiss temperature θ_{CW} in the paramagnetic (PM) regime. These are $\mu_{\text{eff}} = 3.70(3)\mu_B$ and $\theta_{\text{CW}} = -362\text{K}$, for $\text{BaTi}_{1/2}\text{Mn}_{1/2}\text{O}_3$, and $\mu_{\text{eff}} = 4.24(1)\mu_B$ and $\theta_{\text{CW}} = -66\text{K}$, for $\text{Ba}_{0.9}\text{La}_{0.1}\text{Ti}_{1/2}\text{Mn}_{1/2}\text{O}_3$ compound. Both χ_{DC} data were normalized per mol of Mn atoms.

The determined values of θ_{CW} suggest the existence of antiferromagnetic interactions in both systems. For the $x=0$ sample, μ_{eff} is very close to the theoretical estimate for a system of non-interacting Mn^{4+} (d^3) ions, assuming a spin-only system (i.e. $3.87\mu_B$ ²¹). As for the substituted $x=0.1$ sample, the situation is more involved since one expects the bulk susceptibility will contain a contribution from exchange-coupled Mn^{3+} - Mn^{4+} spins added to the contribution from the spins of the secondary phase. It is sufficient now to say (see the next section for more details) that the obtained value is compatible with this picture since it lies between the limits set by the theoretical estimates for a Mn^{4+} and Mn^{3+} spin-only systems.²¹ Furthermore, it is shown that χ_{DC} for $\text{Ba}_{0.9}\text{La}_{0.1}\text{Ti}_{1/2}\text{Mn}_{1/2}\text{O}_3$ presents a clear anomaly at $T \approx 5\text{K}$ in the field-warming regime, likely due to the onset of antiferromagnetic (AFM) order induced by the substitution of Ba by La.

This ordering process, as well as the overall spin dynamics of the Mn ions in both samples, should also be reflected in the evolution of the ESR linewidth ΔH [Figs 5(a)-(b)]. For $\text{BaTi}_{1/2}\text{Mn}_{1/2}\text{O}_3$ (Fig. 5(a)), ΔH undergoes a weak broadening with lowering the temperature

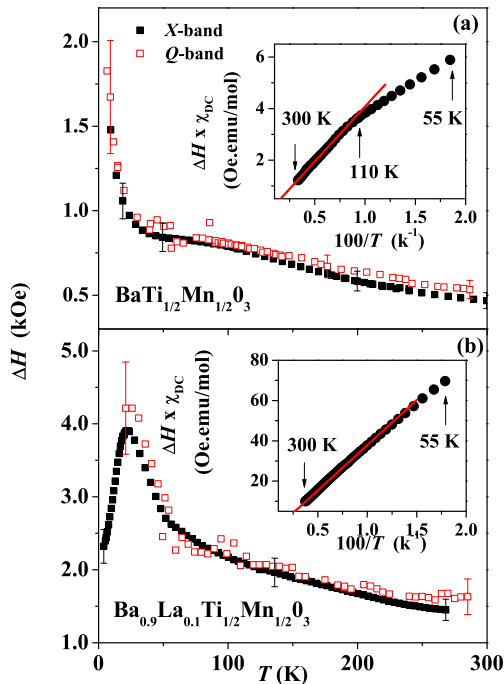


Figure 5: (color online) a) X-band and Q-band linewidth (ΔH) for $\text{BaTi}_{1/2}\text{Mn}_{1/2}\text{O}_3$; b) X-band and Q-band ΔH for $\text{Ba}_{0.9}\text{La}_{0.1}\text{Ti}_{1/2}\text{Mn}_{1/2}\text{O}_3$. In the inset of both figures, it is shown $\Delta H \times \chi_{\text{DC}}$ plotted against $100/T$ (ΔH taken at X-band). The arrow close to $T = 110$ K call the attention for a “kink” in the data. The arrows at $T = 300$ K and $T = 50$ K only indicate the temperature interval being displayed. The solid line is the linear fitting of the data.

from $T = 300$ K down to $T \approx 25$ K, at which a fast broadening process take place down to 4.2 K. For the $x = 0.1$ sample (Fig. 5(b)), one can observe a continuous broadening of ΔH culminating in the peak at $T \approx 25$ K. This observation is another strong suggestion of AFM ordering in the sample. In both Figs. 5(a)-(b), we show that the ΔH measured at Q-band is about the same as the ΔH measured at X-band. This result shows that there are no significant contributions to the ESR spectra originated from sample inhomogeneities. This is of special interest for the $x = 0.1$ sample, since one could expect an inhomogeneous contribution to the ΔH of this sample from the secondary phase observed by the X-rays experiments.

In the inset of both figures, we show $\Delta H \times \chi_{\text{DC}}$ plotted against $100/T$. It has been shown that the temperature evolution of ΔH in strongly coupled transition-metal oxides should follow the Kubo-Tomita formula:^{22,23}

$$\Delta H(T) = \frac{\chi_0(T)}{\chi_{\text{DC}}(T)} \Delta H_{\infty} \quad (1)$$

where $\chi_0(T) = C/T$ denotes the Curie susceptibility (C is the Curie constant) and ΔH_{∞} is a temperature independent parameter to be identified with the high-temperature limit of the ESR linewidth. This expression

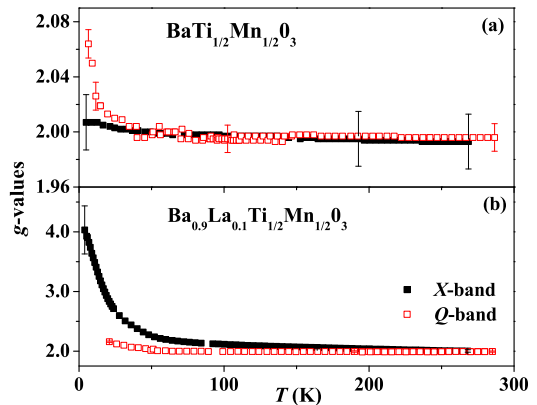


Figure 6: (color online) a) X-band and Q-band g -values for $\text{BaTi}_{1/2}\text{Mn}_{1/2}\text{O}_3$. b) X-band and Q-band g -values for $\text{Ba}_{0.9}\text{La}_{0.1}\text{Ti}_{1/2}\text{Mn}_{1/2}\text{O}_3$.

shows that for a system of uncorrelated spins, for which $\chi_0 = \chi_{\text{DC}}$, ΔH should be constant and would be entirely determined by microscopic parameters of the system. This formula is supposed to hold away from the critical regions of magnetic and structural transitions. Hence, in the light of the above discussions (Fig. 4), we only show the data in the region $T \geq 50$ K. It is noteworthy that the scheme works quite well for $\text{Ba}_{0.9}\text{La}_{0.1}\text{Ti}_{1/2}\text{Mn}_{1/2}\text{O}_3$ but not for $\text{BaTi}_{1/2}\text{Mn}_{1/2}\text{O}_3$, where a “kink” in the data is indicated by the arrow at $T = 110$ K. The parameters extracted from the fitting represented by the solid line are $\Delta H_{\infty} = 227.4$ Oe for $\text{BaTi}_{1/2}\text{Mn}_{1/2}\text{O}_3$, which is rather low if compared with other results in the literature, and $\Delta H_{\infty} \approx 2000$ Oe for $\text{Ba}_{0.9}\text{La}_{0.1}\text{Ti}_{1/2}\text{Mn}_{1/2}\text{O}_3$, which is in the same order of magnitude usually found for a spin resonance arising from Mn^{3+} - Mn^{4+} exchange coupled spins.^{5,6,8}

Another interesting parameter one should take into account are the ESR g -values, since it is sensitive to local internal fields. In Figs. 6(a)-(b) we present the results for the $\text{BaTi}_{1/2}\text{Mn}_{1/2}\text{O}_3$ and $\text{Ba}_{0.9}\text{La}_{0.1}\text{Ti}_{1/2}\text{Mn}_{1/2}\text{O}_3$, respectively. $\text{BaTi}_{1/2}\text{Mn}_{1/2}\text{O}_3$ shows a timid increase of the X-band g -values at low temperatures and a much more conspicuous increase of the Q-band g -values. For $\text{Ba}_{0.9}\text{La}_{0.1}\text{Ti}_{1/2}\text{Mn}_{1/2}\text{O}_3$, on the other hand, both X-band and Q-band g -values increase continuously as the temperature is lowered. The high temperature values measured for both samples are nearly the same ($g = 1.99(1)$) and are expected for transition-metal ions with less than half-filled d -shell. The increase at lower temperatures are most likely due to the internal fields associated with the onset of magnetic order and/or strong magnetic fluctuations.

IV. DISCUSSION

In the preceding section we presented results from X-rays, χ_{DC} and ESR for $\text{BaTi}_{1/2}\text{Mn}_{1/2}\text{O}_3$ suggest-

ing: i) high sample quality, ii) strong AFM interactions, iii) a rather low value of $\Delta H_\infty = 227$ Oe; and for $\text{Ba}_{0.9}\text{La}_{0.1}\text{Ti}_{1/2}\text{Mn}_{1/2}\text{O}_3$ that: i) the substitution of Ba^{2+} by La^{3+} in the A-site of simple perovskite ABO_3 induces AFM order, ii) there is no inhomogeneous contribution to the Mn spin dynamics, iii) $\Delta H_\infty \approx 2000$ Oe, which is compatible with a resonance arising from Mn^{3+} - Mn^{4+} exchange coupled spins. In this section, we further explore these results.

The XRD results at room temperature confirm that substituting La^{3+} for Ba^{2+} in $\text{Ba}_{0.9}\text{La}_{0.1}\text{Ti}_{1/2}\text{Mn}_{1/2}\text{O}_3$ increases the unit cell volume and one must expect symmetry changes as the larger Mn^{3+} ion is present in the structure. From Table I, $M(1)$ - $M(2)$ (between the centers of the face-shared octahedra) and $M(2)$ - $M(3)$ (between the centers of the corner-shared octahedra) as well as the angles $M(1)$ -O- $M(2)$ and $M(2)$ -O- $M(3)$ do not change when comparing both compounds. As BVS calculations show, Mn^{3+} ions (larger) are preferably allocated in the $M(3)$ sites (in the center of the corner-shared octahedron) sharing with Ti^{4+} ions, whereas smaller Mn^{4+} occupy $M(1)$ and $M(2)$ sites (center of the face-shared octahedra). In this situation Mn^{3+} and Mn^{4+} orbitals exchange t_{2g} electrons through O- $2p$ orbitals at the corner-sharing octahedra which may favor the AFM anomaly observed at lower temperatures in the FC-ZFC curves of Fig. 4. A more detailed crystallographic study of these compounds, together with the structural details obtained for other lanthanum concentrations, is being prepared and will be published elsewhere.²⁴

Turning now to the magnetic properties, in the case of $\text{BaTi}_{1/2}\text{Mn}_{1/2}\text{O}_3$ the magnetism arise from Mn^{4+} ions in a $3d^3$ configuration. This configuration has a Hund ground state described by a 4F term. In an octahedral environment, this term splits giving rise to a 4A_2 ground state, which is a non-degenerate orbital angular moment state, i.e. the orbital moment is completely quenched by symmetry requirements. Further lowering of the symmetry does not change this picture. Without a zero field splitting and spin-orbit coupling, one expects that the relaxation process of this system should be quite slow and determined solely by the collective spin motion of the system, the so called bottleneck. This may explains the low value of ΔH_∞ and suggest that the fast broadening of $\Delta H(T)$ for $T \leq 25$ K is due to some change in the spin dynamics of the system.

In order to be more quantitative, we consider the Anderson-Weiss molecular theory,²⁵ which allows one to evaluate a rough estimate of the microscopic parameters of the system. In this model, ΔH_∞ is given by:

$$\Delta H_\infty = \frac{\hbar}{g\mu_B} \frac{\langle \nu_{an}^2 \rangle}{\nu_{ex}} \quad (2)$$

where $\langle \nu_{an}^2 \rangle$ stands for the distribution of the second moment of the resonance due to any anisotropic interaction and ν_{ex} denotes the exchange frequency between the Mn spins. The latter can be estimated from the value of θ_{CW} ,

by using the Weiss molecular-field approximation, and the former was comprehensively studied by Huber *et al.*,⁸ in the context of manganites. Since the 4A_2 ground state is an $L = 0$ state, crystal field effects should be negligible. Therefore, the bulk of ΔH_∞ is determined by dipolar broadening, which contributes with just few Gauss, and by the antisymmetric superexchange (Dzialozhinsky-Moriya, DM) interaction. The second moment due to the latter is approximately given by:⁸

$$\langle \nu_{DM}^2 \rangle \approx \frac{32}{9} S(S+1) D_{DM}^2 \quad (3)$$

The obtained D_{DM} is 0.72 K, which is comparable to estimates of this constant for other manganites using ESR and other methods.⁶⁻⁸ Then, it appears that ΔH_∞ is dominated by the value of the exchange constant J . In this scenario, the broadening of the resonance with lowering the temperature is due to the slowing down of the fluctuations. The long range order is prevented to occur due to the presence of magnetic frustration. The field dependence of the low- T behavior of the g -values [Fig. 6(a)] supports this idea that the resonance is coupled to the fluctuations, for at a higher field (Q -band $H_{res} \approx 1.2$ T), the fluctuations are quenched, leading to a more pronounced increase of the g -values.

In principle, the ‘‘kink’’ in the inset of Fig. 5(a) at $T \approx 110$ K point to a crossover of the spin dynamics of the Mn^{4+} ions system. However, we refrain from taking any conclusion since we observed that this is a sample-dependent effect that turned out to be more or less pronounced depending on the sample grounding time during the synthesis. Therefore, we conclude that any intrinsic (sample independent) change in spin dynamics of this system takes place at $T \approx 25$ K, as evidenced by the broadening of the resonance.

For $\text{Ba}_{0.9}\text{La}_{0.1}\text{Ti}_{1/2}\text{Mn}_{1/2}\text{O}_3$ one expect that the charge transfer to Mn^{4+} ions, as implied by the substitution of Ba^{2+} by La^{3+} , gives rise to a Mn^{3+} - Mn^{4+} exchange coupled system. The obtained effective moment from χ_{DC} agrees with this expectation. Furthermore, an AFM long range order with $T_N = 5$ K is suggested by χ_{DC} . As for the ESR results, the existence of the secondary phase revealed in the XRD data do not give rise to an inhomogeneous contribution to ΔH . The comparison with a copper sulfate standard ($\text{CuSO}_4 \cdot 5\text{H}_2\text{O}$) allows a rather crude estimate of the χ_{ESR} in emu/mol, which in turn allows one to calculate the effective moment as determined by the ESR measurement. In doing that, we obtained $\mu_{eff} = 4.1(5)\mu_B$, that agrees with the results for χ_{DC} .

The onset of long range order is also suggested by the anomaly in ΔH [Fig. 5(b)]. The peaks observed by macroscopic and microscopic measurements differ in the temperatures at which they take place ($T_N = 25$ K for ESR and $T_N = 5$ K for χ_{DC}). The result suggests an investigation of the magnetic properties of the secondary phase $\text{Ba}_{0.4}\text{La}_{0.6}\text{Ti}_{1/2}\text{Mn}_{1/2}\text{O}_3$ ²⁴, which reveals that this peak is due to the critical fluctuations

present in this secondary phase. Therefore, for $T \leq 50$ K, the ESR is dominated by the spin dynamics of the $\text{Ba}_{0.4}\text{La}_{0.6}\text{Ti}_{1/2}\text{Mn}_{1/2}\text{O}_3$ system, whereas for $T \geq 50$ K, it reflects a $\text{Mn}^{3+}/\text{Mn}^{4+}$ exchange coupled spins.

The measured value of $\Delta H_\infty \approx 2000$ Oe is one order of magnitude larger than the value found for the non-doped system, pointing to the emergence of new contributions to the linewidth. In particular, one should consider the second moment given by crystal field effects and some increase in the value of the D_{DM} constant interaction. Nonetheless, previous investigations have argued that D_{DM} does not change significantly along a given series of doped manganites.⁸ According to Eq. 2, the evaluation of crystal field effects requires the knowledge of the second moment distribution due to crystal fields and an estimate for the exchange frequency. As before, the exchange frequency is estimated from the Weiss-molecular field approximation taking into account the existence of two spin species ($S = 3/2$ for Mn^{4+} and $S = 2$ for Mn^{3+}). The second moment from crystal fields reads:⁸

$$\langle \nu_{DM}^2 \rangle = (4/30)(4S(S+1) - 3)D_{CF}^2 \quad (4)$$

The value of $D_{CF} = 2.0 - 5.0$ K is obtained. The error is mainly due to the uncertainty on the fraction of Mn^{3+} and Mn^{4+} as induced by the La-substitution. Certainly, all these estimates must be reviewed by the application of more powerful techniques, such as neutron scattering.

It is interesting to observe the conspicuous increase of the X -band g -values in the case of the $x = 0.1$ sample, as shown in Fig. 6(b). This increase is related with the onset of internal fields which shift the resonance when a phase transition is approached. This time, at relatively higher fields, the increase in g -values is lower. Here, the high field of the Q -band experiment suppresses the AFM transition to lower temperatures, delaying the shift of the resonance. Nonetheless, one should note that the increase of the Q -band g -values, although dwarfed by the huge increase observed in the low field (X -band) experiment, is still larger than the one of the X -band g -values of $\text{BaTi}_{1/2}\text{Mn}_{1/2}\text{O}_3$.

V. SUMMARY

We presented a study of the magnetic properties of the $\text{BaTi}_{1/2}\text{Mn}_{1/2}\text{O}_3$ and $\text{Ba}_{0.9}\text{La}_{0.1}\text{Ti}_{1/2}\text{Mn}_{1/2}\text{O}_3$ com-

pounds in the temperature interval $2\text{K} \leq T \leq 350\text{K}$ using ESR and DC-susceptibility measurements.

For $\text{BaTi}_{1/2}\text{Mn}_{1/2}\text{O}_3$, our results confirmed the existence of strong AFM interactions and, in particular, we have shown that the slowing down of the AFM fluctuations begin to dominate the evolution of the ESR parameters at $T \approx 25$ K. A rather low value of $\Delta H_\infty = 227$ Oe was obtained and related to exchange narrowing effects due to the AFM interactions at high- T . The value of the asymmetric superexchange interaction was estimated to be $D_{DM} = 0.72$ K. It is strongly suggested that long range magnetic order is prevented to occur due to the presence of magnetic frustration.

For $\text{Ba}_{0.9}\text{La}_{0.1}\text{Ti}_{1/2}\text{Mn}_{1/2}\text{O}_3$, a phase transition to an AFM state is suggested by the χ_{DC} and ΔH measurements but at different temperatures ($T_N = 5\text{K}$ for χ_{DC} and $T_N = 25\text{K}$ from the ESR). As given by our quantitative XRD refinement results, a secondary phase was identified for the $x=0.1$ sample which has been ascribed to the presence of the corner-shared octahedra trigonal structure $\text{Ba}_{0.4}\text{La}_{0.6}\text{Ti}_{1/2}\text{Mn}_{1/2}\text{O}_3$ (space group $R\bar{3}c$). We pointed out that for $T \leq 50$ K the ESR captures the spin dynamics of this secondary phase. For $T \geq 50$ K, the measured value of $\Delta H_\infty \approx 2000$ Oe is compatible with what is expected from a resonance arising from a Mn^{3+} - Mn^{4+} exchange-coupled spin system. In this scenario, we evaluated a rough estimate for the crystal field parameter, obtaining $D_{CF} = 2.0 - 5.0\text{K}$. For this compound, the refinement of the XRD data at room temperature, when compared to the XRD data from the non-substituted ($x=0$) sample, reveals no effective changes in bond length between B cations at the face-shared octahedra, nor the angles $M(1)\text{-O-}M(2)$ in the trimers or $M(2)\text{-O-}M(3)$ in the corner-shared dimers are changing. The appearance of an AFM anomaly around 5K in the substituted sample seems to be related with the magnetic exchange between Mn^{4+} and Mn^{3+} at the neighboring $M(2)$ and $M(3)$ sites, respectively.

Acknowledgments

This work was supported by FAPEMIG (MG-Brazil) Grants No. APQ-01577-09, 2010-EXA023 and 2012-EXA011, CNPq (Brazil) Grants 482549/2010-6 and 2010-EXA020.

¹ E. Dagotto, Science **309**, 257 (2005) and references therein.

² A. Pimenov et al., Nature Phys. **2**, 97 (2006); Special issue *J. Phys. Condens. Matter* **20**, 434201-434220 (2008). No. 434209.

³ Daniel Khomskii, "Classifying multiferroics: Mechanisms and effects", Physics **2**, 20 (2009) DOI:

10.1103/Physics.2.20.

⁴ G. M. Keith, C. A. Kirk, K. Sarma, N. M. Alford, E. J. Cussen, M. J. Rosseinsky, and D. C. Sinclair, Chem. Mater. **16**, 2007 (2004).

⁵ M. T. Causa, M. Tovar, A. Caneiro, F. Prado, G. Ibañez, C. A. Ramos, A. Butera, B. Alascio, X. Obradors, S. Piñol,

- et al., Phys. Rev. B **58**, 3233 (1998).
- ⁶ J. Deisenhofer, M. Paraskevopoulos, H.-A. K. von Nidda, and A. Loidl, Phys. Rev. B **66**, 054414 (2002).
 - ⁷ J. Deisenhofer, B. I. Kochelaev, E. Shilova, A. M. Balbashov, A. Loidl, and H.-A. K. von Nidda, Phys. Rev. B **68**, 214427 (2003).
 - ⁸ D. L. Huber, G. Alejandro, A. Caneiro, M. T. Causa, F. Prado, M. Tovar, and S. B. Oseroff, Physical Review B **60**, 12155 (1999).
 - ⁹ N. O. Moreno, P. G. Pagliuso, C. Rettori, J. Gardner, , J. L. Sarrao, J. D. Thompson, D. L. Huber, J. F. Mitchell, J. J. Martinez, et al., Physical Review B **63**, 174413 (2001).
 - ¹⁰ A. Shengelaya, G. meng Zhao H. Keller, and K. A. Müller, Phys. Rev. Lett. **77**, 5296 (1996).
 - ¹¹ A. Shengelaya, G. meng Zha, H. Keller, K. A. Müller, and B. I. Kochelaev, Phys. Rev. B **61**, 5888 (2000).
 - ¹² A.C. Larson and R.B. Von Dreele, *General Structure Analysis System (GSAS)*, Los Alamos National Laboratory Report LAUR 86-748 (2000).
 - ¹³ B. H. Toby, J. Appl. Cryst. **34**, 210 (2001).
 - ¹⁴ Y.-C. Wu, S.-F. Wang, and S.-H. Chen, J. Am. Ceram. Soc. **92**[9], 2099 (2009).
 - ¹⁵ L. Miranda, A. Feteira, D. C. Sinclair, K. Boulahya, M. Hernando, J. Ramírez, A. Varela, J. M. González-Calbet, and M. Parras, Chem. Mater. **21**, 1731 (2009).
 - ¹⁶ Diamond – Crystal and Molecular Structure Visualization Crystal Impact – K. Brandenburg & H. Putz GbR, Rathausgasse 30, D-53111 Bonn.
 - ¹⁷ M. W. Lufaso and P. M. Woodward, Acta Cryst. **B57**, 725 (2001).
 - ¹⁸ J. M. D. Coey, M. Viret, and S. von Molnár, Adv. Phys. **48**, 167 (1999).
 - ¹⁹ J. A. M. van Roosmalen, P. van Vlaanderen, and E. H. P. Cordfunke, J. Sol. State Chem. **114**, 516 (1995).
 - ²⁰ J. P. Joshi and S. V. Bhat, J. Magn. Reson. **168**, 284 (2004).
 - ²¹ N. W. Ashcroft and N. D. Mermin, *Solid State Physics* (Brooks/Cole, Florence, KY 41022-6904, 1976), pp. 657-659.
 - ²² D. L. Huber, Phys. Rev. B **12**, 31 (1975).
 - ²³ D. L. Huber, Phys. Rev. B **13**, 291 (1976).
 - ²⁴ R. Lora-Serrano, F. A. Garcia, P. Marques-Ferreira, J. G. S. Duque *et al.*, In preparation.
 - ²⁵ P. W. Anderson and P. R. Weiss, Rev. Mod. Phys. **25**, 269 (1953).